Shedding Light on Excited-State Structures by Theoretical Analysis of Femtosecond Transient Infrared Spectra: Intramolecular Charge Transfer in 4-(Dimethylamino)benzonitrile

Jens Dreyer* and Andreas Kummrow

Contribution from the Max-Born-Institut für Nichtlineare Optik und Kurzzeitspektroskopie, Max-Born-Strasse 2A, 12489 Berlin, Germany

Received June 21, 1999. Revised Manuscript Received January 12, 2000

Abstract: We performed a detailed theoretical analysis of femtosecond transient infrared spectra to determine excited-state structures involved in photoinduced intramolecular charge transfer (ICT) in 4-(dimethylamino)-benzonitrile (DMABN). For comparison, 4-aminobenzonitrile (ABN) is studied. We present the first ab initio CASSCF study with all states under consideration being fully optimized. We derive two different models for the locally excited (LE) states: a planar and a novel pyramidal conformation. Three different mechanisms are treated for the ICT state formation: the twisted ICT (TICT), the pseudo-Jahn−Teller ICT (PICT), and the rehybridized ICT (RICT) models. By use of this combined theoretical and experimental approach, we can evaluate the respective models and thus provide new insight into the ICT process. We assign a pyramidal LE state to ABN, and, in contrast, a planar LE state to DMABN. We can conclusively rule out RICT as the ICT mechanism in DMABN. Although our results favor TICT as the ICT mechanism in DMABN, a final statement cannot be made. We predict, however, that determination of the position of the, as yet, unobserved phenyl−amino stretching vibration will substantiate a definitive explanation of the ICT mechanism in DMABN.

1. Introduction

Recent development of femtosecond time-resolved spectroscopy has enabled the investigation of ultrafast photochemical reactions.[1] Absorption and fluorescence techniques are widely used in this context. They provide valuable insight into reaction dynamics, but only limited information on molecular structures. Thus, reliable knowledge about molecular structures associated with short-lived intermediates in photochemical reactions is still rare. Femtosecond time-resolved vibrational spectroscopy is clearly superior to this approach, because it gives information not only on dynamics but also on structural characteristics of the molecule in the course of the reaction.[2] Variations in frequency and intensity of the bands can already give hints about structural changes evolving during the chemical reaction. However, complete structural resolution from experimental infrared spectra alone cannot be expected, not even for medium-sized molecules.

Substantial progress in theoretical methods, in particular complete active space self-consistent field (CASSCF) calculations, has been achieved in elucidating photochemical reactions.[3] But frequently, such calculations yield several different models or mechanisms with competitive pathways, the evaluation of which solely based upon theoretical results is generally impossible. Thus, the allocation of excited-state structures and information about photochemical reaction mechanisms can only be successfully obtained by experimental and theoretical efforts in conjunction. Therefore, we introduce the combined approach of femtosecond infrared spectroscopy and ab initio CASSCF calculations of excited-state structures and vibrational patterns to study photochemical reactions.

The nature of excited states involved in photoinduced intramolecular charge transfer (ICT) reactions is a matter of considerable and current dispute.[4] A prototype is the ICT reaction in photoexcited 4-(dimethylamino)benzonitrile (DMABN, Chart 1). A remarkable feature of this reaction is the occurrence of dual fluorescence, which was discovered 40 years ago.[5,6] Obviously more than one transient species is formed during the reaction. It has been established that the short-axis-polarized normal fluorescence band (L_b-type) arises from a moderately polar locally excited (LE) state. The long-axis-polarized and red-shifted anomalous band (L_a-type) has its source in a highly polar charge-transfer (CT) state. Since its initial discovery, dual fluorescence has been found in a variety of other donor−acceptor compounds with the two moieties linked by a single bond.[7−19] Fluorescence decay measurements demonstrated that

* Corresponding author. E-mail: dreyer@mbi-berlin.de. Fax: +49 30 6392 1429.

(1) *Femtosecond Chemistry*; Manz, J., Wöste, L., Eds.; VCH: New York, 1995.

(2) Elsaesser, T. In *Femtosecond Chemistry*; Manz, J., Wöste, L., Eds.; VCH: New York, 1995; pp 563−579.

(3) Klessinger, M.; Michl, J. *Excited States and Photochemistry of Organic Molecules*; VCH: New York, 1995.

(4) Rettig, W.; Bliss, B.; Dirnberger, K. *Chem. Phys. Lett.* **1999**, *305*, 8−14.

(5) Lippert, E.; Lüder, W.; Moll, F.; Nägele, W.; Boos, H.; Prigge, H.; Seibold-Blankenstein, I. *Angew. Chem.* **1961**, *73*, 695−706.

(6) Lippert, E.; Lüder, W.; Boos, H. In *Advances in Molecular Spectroscopy*; Mangini, A., Ed.; Pergamon Press: Oxford, 1962; pp 443−457.

(7) Rotkiewicz, K.; Grellmann, K. H.; Grabowski, Z. R. *Chem. Phys. Lett.* **1973**, *19*, 315−318.

(8) Rotkiewicz, K.; Grellmann, K. H.; Grabowski, Z. R. *Chem. Phys. Lett.* **1973**, *21*, 212.

(9) Rettig, W. *Angew. Chem., Int. Ed. Engl.* **1986**, *25*, 971−988.

(10) Lippert, E.; Rettig, W.; Bonacic-Koutecký, V.; Heisel, F.; Miehé, J. A. *Adv. Chem. Phys.* **1987**, *68*, 1−173 and references therein.

(11) Rettig, W. In *Topics in Current Chemistry, Electron-Transfer I*; Mattay, J., Ed.; Springer: Berlin, 1994; Vol. 169, pp 253−299.

(12) Leinhos, U.; W. Kühnle, W.; Zachariasse, K. A. *J. Phys. Chem.* **1991**, *95*, 2013−2021.

10.1021/ja992095e CCC: $19.00
Published on Web 03/04/2000

Chart 1

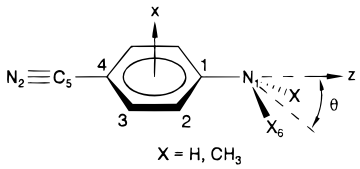

a small energy gap between the interacting states is an essential prerequisite for the ICT process in these molecules.

A multitude of experimental[4−19] and theoretical gas-[20−26] and solution-phase[27−36] studies on the nature of the ICT process in DMABN have been published. None of them was able provide conclusive evidence for excited-state structures. Some indication of the gas-phase structure of the LE states of DMABN[37,38] and 4-aminobenzonitrile (ABN, Chart 1)[39] has been gained by rotationally resolved fluorescence. The LE state of DMABN is supposed to be 30° twisted with a planar amino group.[37] This is in accord with a Franck−Condon intensity analysis of mass-resolved excitation spectra.[40] The phenyl−amino and phenyl−cyano bond lengths are expected to decrease upon excitation.[37] However, recent fluorescence excitation experiments under isolated, supercooled conditions indicate that DMABN is planar in the LE state.[38]

Chart 2

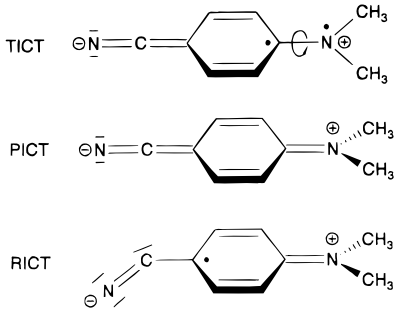

ABN does not exhibit dual fluorescence, neither in solution nor in the gas phase, and hence does not undergo charge transfer.[12,13] Rotationally resolved excitation spectra indicated that the pyramidalization of the amino group as well as the untwisted conformation remain unchanged upon excitation.[39] The experimental findings are consistent with an expanded benzene ring with the four C−C bonds adjacent to the substituents increasing more than the remaining two C−C bonds, a contracted phenyl−amino bond and a slightly reduced C≡N bond length. Further information on LE structures has been obtained by semiempirical[27,32,33] and ab initio calculations, using CI singles (CIS).[25]

In recent times the discussion about the nature of the CT state of DMABN has been concentrated on three different models (Chart 2). Within the twisted ICT (TICT) model[7,8] the charge separation in the CT state is supposed to result from complete decoupling between the amino and benzonitrile moieties by twisting the amino group into a perpendicular position. [4,7−11]

Solvent-induced vibronic coupling of the LE and CT states is assumed in the pseudo-Jahn−Teller model to form a conjugated planar CT (PICT) state.[12−17] The coupling is supposed to be mediated by the amino group inversion mode. The PICT model implies that planarization of the initially pyramidalized molecule corresponds to the rate-determining step in the ICT reaction. In contrast to assumptions underlying the TICT model, the amino and benzonitrile moieties are strongly coupled in the PICT state.

The pseudo-Jahn−Teller model has also been interpreted as a change from planar sp^2 to pyramidal sp^3 hybridization of the amino nitrogen, inducing a decoupling of the nitrogen lone pair from the benzene ring, thereby increasing the charge separation (wagged ICT model, WICT).[13,14] However, by calculating potential energy surfaces along the wagging coordinate it was shown that the increase of the inversion angle is unable to produce the required highly polar state.[20,21,26,27,33] Thus the WICT model is not considered further here.

Rehybridization of the cyano carbon atom from sp to sp^2 entailing a bent cyano bond is the key feature of the rehybridized ICT (RICT) model, which was deduced from results of ab initio CIS optimizations by identifying a corresponding excited-state minimum.[22−24]

Recently, the first femtosecond UV pump midinfrared probe study on DMABN and ABN in acetonitrile has been presented.[41] Transient infrared absorption spectra with striking differences for the LE states of DMABN and ABN as well as a transient spectrum for the CT state of DMABN have been reported.[41] Understanding the features of the transient infrared spectra is a key to resolve excited-state structures and the ICT mechanism.

(13) Schuddeboom, W.; Jonker, S. A.; Warman, J. H.; Leinhos, U.; Kühnle, W.; Zachariasse, K. A. *J. Phys. Chem.* **1992**, *96*, 10809−10819.
(14) Zachariasse, K. A.; von der Haar, T.; Hebecker, A.; Leinhos, U.; Kühnle, W. *Pure Appl. Chem.* **1993**, *65*, 1745−1750.
(15) von der Haar, T.; Hebecker, A.; Il'ichev, Y. V.; Jiang, Y.-B.; Kühnle, W.; Zachariasse, K. A. *Recl. Trav. Chim. Pays-Bas.* **1995**, *114*, 430.
(16) Zachariasse, K. A.; Grobys, M.; von der Haar, T.; Hebecker, A.; Il'ichev, Y. V.; Jiang, Y.-B.; Morawski, O.; Kühnle, W. *J. Photochem. Photobiol. A: Chem.* **1996**, *102*, 59−70.
(17) Il'ichev, Y.; Kühnle, W.; Zachariasse, K. A. *J. Phys. Chem. A* **1998**, *102*, 5670−5680.
(18) Changenet, P.; Plaza, P.; Martin, M. M.; Meyer, Y. H. *J. Phys. Chem. A* **1997**, *101*, 8186−8194.
(19) Su, S.-G.; Simon, J. D. *J. Chem. Phys.* **1988**, *89*, 908−919.
(20) Sudholt, W.; Sobolewski, A.; Domcke, W. *Chem. Phys.* **1999**, *250*, 9−18 and references therein.
(21) Serrano-Andrés, L.; Merchan, M.; Roos, B. O.; Lindh, R. *J. Am. Chem. Soc.* **1995**, *117*, 3189−3204.
(22) Sobolewski, A.; Domcke, W. *Chem. Phys. Lett.* **1996**, *259*, 119−127.
(23) Sobolewski, A.; Domcke, W. *Chem. Phys. Lett.* **1996**, *250*, 428−436.
(24) Sobolewski, A.; Sudholt, W.; Domcke, W. *J. Phys. Chem. A* **1998**, *102*, 2716−2722.
(25) Lommatzsch, U.; Brutschy, B. *Chem. Phys.* **1998**, *234*, 35−57.
(26) Parusel, A. B. J.; Köhler, G.; Grimme, S. *J. Phys. Chem. A* **1998**, *102*, 6297−6306.
(27) Gedeck, P.; Schneider, S. *J. Photochem. Photobiol. A: Chem.* **1997**, *105*, 165−181 and references therein.
(28) Moro, G. J.; Nordio, P. L.; Polimeno, A. *Mol. Phys.* **1989**, *68*, 1131−1141.
(29) Kato, S.; Amatatsu, Y. *J. Chem. Phys.* **1990**, *92*, 7241−7257.
(30) Fonseca, T.; Kim, H. J.; Hynes, J. T. *J. Mol. Liq.* **1994**, *60*, 161−200.
(31) Fonseca, T.; Kim, H. J.; Hynes, J. T. *J. Photochem. Photobiol. A* **1994**, *82*, 67−79.
(32) Broo, A.; Zerner, M. C. *Theor. Chim. Acta* **1995**, *90*, 383−395.
(33) Gorse, A.-D.; Persquer, M. *J. Phys. Chem.* **1995**, *99*, 4039−4049.
(34) Soujanya, T.; Saroja, G.; Samanta, A. *Chem. Phys. Lett.* **1995**, *236*, 503−509.
(35) Hayashi, S.; Ando, K.; Kato, S. *J. Phys. Chem.* **1995**, *99*, 955−964.
(36) Kim, H. J.; Hynes, J. T. *J. Photochem. Photobiol. A* **1997**, *105*, 337−343.
(37) Kajimoto, O.; Yokoyama, H.; Ooshima, Y.; Endo, Y. *Chem. Phys. Lett.* **1991**, *179*, 455−459.
(38) Pérez Salgado, F.; Herbich, J.; Kunst, A. G. M.; Rettschnick, R. P. H. *J. Phys. Chem. A* **1999**, *103*, 3184−3192.
(39) Berden, G.; van Rooy, J.; Meerts, W. L.; Zachariasse, K. A. *Chem. Phys. Lett.* **1997**, *278*, 373−379.
(40) Grassian, V. H.; Warren, J. A.; Bernstein, E. R. *J. Chem. Phys.* **1989**, *90*, 3994−3999.
(41) Chudoba, C.; Kummrow, A.; Dreyer, J.; Stenger, J.; Nibbering, E. T. J.; Elsaesser, T.; Zachariasse, K. A. *Chem. Phys. Lett* **1999**, *309*, 357−363.

This article gives a detailed theoretical analysis of the recently published experimental results.[41] It is the first ab initio CASSCF study with all states under consideration being fully optimized. We present two potential structures for the LE states of ABN and DMABN, a planar and a novel pyramidal conformation. Results are obtained for all CT models under consideration. In particular we will show that the individual optimization of the planar L_a-type state ($2A_1$) of DMABN yields a conjugated PICT state with high polarity. Implications for the ICT mechanism will be discussed in the light of the present combined experimental and theoretical results.

2. Computational Methods

The CASSCF methods implemented in the program packages GAUSSIAN94/98 and MOLPRO96/98 have been applied for all calculations.[42,43] The 6-31G(d) basis set with polarization functions on heavy atoms was used throughout.[44,45] To keep geometry optimizations and vibrational normal-mode analyses affordable, the active space was restricted to four electrons distributed over four orbitals for nontwisted structures (4e/4o). These are the highest occupied and unoccupied a_2 (a'') and b_1 (a') orbitals in the C_{2v} (C_s) point group (cf. Figure 3). For 90°-twisted conformations (TICT) the doubly occupied lone pair orbital of the amino nitrogen, which has b_2 (a'') symmetry, has been added (6e/5o).

Single-point calculations have been performed with extended active spaces, which included all benzene π orbitals combined with the amino nitrogen lone pair orbital as well as the cyano π_{yz} and π_{xz} orbitals (12e/11o). These results show, in agreement with previously reported calculations, that the small active space chosen for geometry optimization and vibrational analyses ensures a qualitatively correct description of the electronic wave function and the geometry.[20−24,26]

Vibrational frequencies have been calculated analytically (cpu time $\approx$ 10 h on SGI Origin 2000/2 Gb RAM) as well as numerically (cpu time $\approx$ 40 h), showing only small deviations. CASSCF infrared intensities are available only by numerical differentiation. To be consistent, all reported frequencies have been taken from numerical calculations and were scaled by the standard factor of 0.9.[46] The step size for numerical differentiation has been varied from the default value of 0.5 pm down to 0.1 pm. Usually intermediate values were found to produce reasonable results. In some cases, other settings resulted in artifacts, i.e., imaginary frequencies, which are absent with analytical gradients, or unreasonably high frequencies and intensities. Numerically calculated frequencies turn out to be rather stable with regard to the choice of parameters for numerical vibrational analysis.

Sensitivity of calculated infrared intensities to various parameters is a well-documented phenomenon.[47] However, it has been shown that qualitative features of the infrared spectrum, such as the order and approximate ratio of intensities, are correctly predicted if at least split-valence polarized basis sets, such as the one used here, are applied, whereas absolute values may deviate.[48]

Table 1. Ground-State Geometries for ABN: Point Group and State Symmetries, Dipole Moments μ (in D), Bond Lengths (in pm), Pyramidalization Angle θ (Chart 1), and Sum of Bond Angles at the Amino Nitrogen Atom

	CAS(4e,4o)/ 6-31G(d)[a]	CAS(12e,9o)/ DZP[b]	B3LYP/ 6-31G(d)[c]	exptl[d]
symmetry	C_s: 1A′	C_{2v}: $1A_1$	C_s: 1A′	C_s: 1A′
μ	6.0	6.9	6.8	6.6[e]
N_1-C_1	139.1	136.7	138.5	137.0
C_1-C_2	139.3	139.9	140.9	140.5
C_2-C_3	138.6	139.1	138.6	136.9
C_3-C_4	139.6	139.9	140.7	139.8
C_4-C_5	144.4	144.6	143.0	143.1
C_5-N_2	113.6	115.8	116.5	114.8
$C_2C_1N_1H_3$	25.6°	0.0°		
θ	41.6°	0.0°	34°	34°
Σ(N-angle)	341.2°	360.0°	341.7°	346°

[a] This work. [b] Reference 21. [c] Reference 25. [d] X-ray crystal structure, ref 52. [e] Dipole moment in 1,4-dioxane (25 °C), ref 13.

Dynamical electron correlation is well known to have a marked effect on energies.[20−24] Algorithms taking dynamical correlation effects into account are not yet available for CASSCF optimizations and calculations of infrared spectra. However, geometries are expected to be much less sensitive to the level of theory than energy calculations.

Molecular properties such as geometries, dipole moments, vibrational spectra, and normal modes can be altered in polar solvents[49] such as acetonitrile, which was used in the femtosecond transient infrared study.[41] The influence of polar solvation on the dipole moment of DMABN was estimated from AM1-CI reaction field calculations by Gedeck and Schneider.[27] They found that the dipole moments are increased in going from the gas phase to acetonitrile from 5.7 to 7.3 D for the ground state, from 11.8 D (in diethyl ether) to 12.5 D for the LE state, and from 14.8 to 15.9 D for the TICT state. This moderate increase suggests that the effect on geometries is also of minor importance. Ground-state vibrational frequency shifts for the vibrational modes under consideration between the gas phase or unpolar solvents (CCl_4), respectively, and the polar solvent acetonitrile are less than 5 cm^{-1} for ABN and DMABN.[50,51] This indicates that the relevant molecular properties of ABN and DMABN are not changed considerably by polar solvation, and, therefore, that the vibrational spectra are reasonably described by gas-phase calculations for these molecules.

3. Results

3.1. Ground State. Optimized ground-state geometries of ABN and DMABN are in good agreement with X-ray crystal structures as well as results from previously reported calculations (Tables 1 and 2). The numbering of atoms is given in Chart 1. A comparison of geometries for ground and excited states is depicted in Figure 1 for ABN and in Figure 2 for DMABN. It has been shown by previous computational studies that the resulting angle of pyramidalization (inversion angle) of the amino group θ (Chart 1) strongly depends on the theoretical level.[23,25] The CAS(4e,4o)/6-31G(d) approach employed in this work calculates the inversion angle in ABN to 41.6° and to 22.2° in DMABN, which are slightly larger than known experimental values of 34° for ABN and 11.9° and 15°, respectively, for DMABN.[37,52] Accordingly, the N_1-C_1 bond

(42) Frisch, M. J.; Trucks, G. W.; Schlegel, H. B.; Scuseria, G. E.; Robb, M. A.; Cheeseman, J. R.; Zakrzewski, V. G.; Montgomery, J. A.; Stratmann, R. E.; Burant, J. C.; Dapprich, S.; Millam, J. M.; Daniels, A. D.; Kudin, K. N.; Strain, M. C.; Farkas, O.; Tomasi, J.; Barone, V.; Cossi, M.; Cammi, R.; Mennucci, B.; Pomelli, C.; Adamo, C.; Clifford, S.; Ochterski, J.; Petersson, G. A.; Ayala, P. Y.; Cui, Q.; Morokuma, K.; Malick, D. K.; Rabuck, A. D.; Raghavachari, K.; Foresman, J. B.; Cioslowski, J.; Ortiz, J. V.; Stefanov, B. B.; Liu, G.; Liashenko, A.; Piskorz, P.; Komaromi, I.; Gomperts, R.; Martin, R. L.; Fox, D. J.; Keith, T.; Al-Laham, M. A.; Peng, C. Y.; Nanayakkara, A.; Gonzalez, C.; Challacombe, M.; Gill, P. M. W.; G. Johnson, B.; Chen, W.; Wong, M. W.; Andres, J. L.; Head-Gordon, M.; Replogle E. S.; Pople, J. A. *Gaussian 98 (Revision A.2)*; Gaussian, Inc.; Pittsburgh, PA, 1998.

(43) MOLPRO (Version 96.4) is a package of ab initio programs written by Werner, H.-J. and. Knowles, P. J., with contributions by Almlöf, J.; Amos, R.; Berning, A.; Deegan, M. J. O.; Eckert, F.; Elbert, S. T.; Hampel, C.; Lindh, R.; Meyer, W.; Nicklass, A.; Peterson, K.; Pitzer, R.; Stone, A. J.; Taylor, P. R.; Mura, M. E.; Pulay, P.; Schuetz, M.; Stoll, H.; Thorsteinsson, T.; and Cooper, D. L.

(44) Hehre, W. J.; Ditchfield, R.; Pople, J. A. *J. Chem. Phys.* **1972**, *56*, 2257−2261.

(45) Harihan, P. C.; Pople, J. A. *Theor. Chim. Acta* **1973**, *28*, 213−222.

(46) Scott, A.; Radom, L. *J. Phys. Chem.* **1996**, *100*, 16502−16513.

(47) Galabov, B.; Bobadova-Parvanova, P.; Dudev, T. *J. Mol. Struct.* **1997**, *406*, 119−125.

(48) Yamaguchi, Y.; Frisch, M.; Gaw, J.; Schaefer, H. F., III; Binkley, J. S. *J. Chem. Phys.* **1986**, *84*, 2262−2278−2278.

(49) Cramer, C. J.; Truhlar, D. G. *Chem. Rev.* **1999**, *99*, 2161−2200.

(50) Ram, S.; Yadav, J. S.; Rai, D. K. *Ind. J. Phys.* **1985**, *59B*, 19−28.

(51) Gates, P. N.; Steele, D.; Pearce, R. A. R.; Radcliffe, *K. J. Chem. Soc., Perkin Trans. 2* **1972**, 1607−1613.

(52) Heine, A.; Herbst-Irmer, R.; Stalke, D.; Kühnle, W.; Zachariasse, K. A. *Acta Crystallogr.* **1994**, *B50*, 363−373.

Table 2. Ground-State Geometries for DMABN: Point Group and State Symmetries, Dipole Moments μ (in D), Bond Lengths (in pm), Pyramidalization Angle θ (Chart 1), and Sum of Bond Angles at the Amino Nitrogen Atom

	CAS(4e,4o)/ 6-31G(d)[a]	CAS(12e,9o)/ DZP[b]	B3LYP/ cc-pVDZ[c]	exptl[d]
symmetry	C_s: 1A′	C_s: 1A′	C_{2v}: $^1A_1$	C_s: 1A′
μ	6.6	6.4	7.5	6.6[e]
N_1-C_1	138.6	138.8	137.7	136.7
C_1-C_2	140.1	140.6	142.0	140.0
C_2-C_3	138.5	139.1	138.8	137.0
C_3-C_4	139.4	139.9	140.7	138.8
C_4-C_5	144.4	144.6	143.2	143.4
C_5-N_2	113.7	115.7	116.6	114.5
N_1-C_6	144.7	146.0	145.2	145.6
$C_2C_1N_1C_6$	13.6°	21.2°	0.0°	
θ	22.2°		0.0°	11.9°, 15°[f]
Σ(N-angle)	354.9°		360.0°	358.5°

[a] This work. [b] Reference 21. [c] Reference 25. [d] X-ray crystal structure, ref 52. [e] Dipole moment in 1,4-dioxane (25 °C), ref 13. [f] Reference 37.

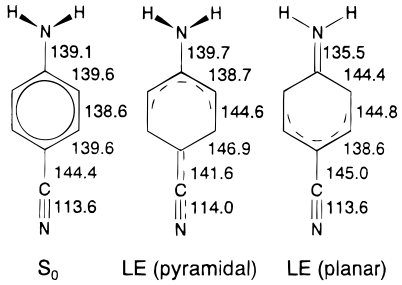

Figure 1. CASSCF-optimized geometries for ABN, with bond lengths in picometers.

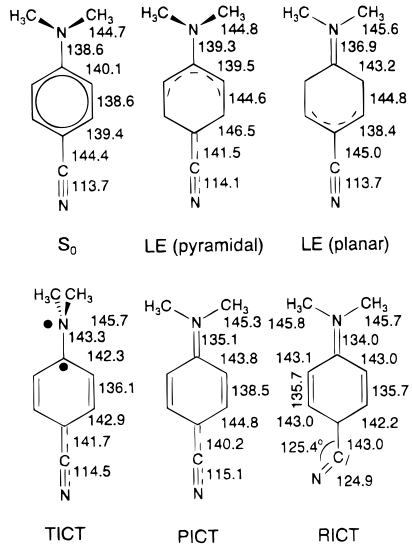

Figure 2. CASSCF-optimized geometries for DMABN, with bond lengths in picometers.

lengths turn out to be somewhat longer in comparison to crystal structure values due to the lower degree of conjugation between the nitrogen lone pair and the phenyl ring. This entails underestimated force constants and vibrational frequencies, which are somewhat too low in comparison to experimental values (vide infra). The strength of the cyano triple bond is overestimated and turns out to be a little too short with respect to crystal structure values. It should be noted that Serrano-Andrés et al. suggested that the measured C_2-C_3 bond lengths are too small.[21]

Table 3. Locally Excited (LE)-State Geometries for ABN: Point Group and State Symmetries, Dipole Moments μ (in D), Bond Lengths (in pm), Pyramidalization Angle θ (Chart 1), and Sum of Bond Angles at the Amino Nitrogen Atom

	CAS(4e,4o)/6-31G(d)		CIS/cc-pVDZ, LE (planar)[b]
	LE (pyramidal)[a]	LE (planar)[a]	
symmetry	C_s: 1A″	C_{2v}: $^1B_2$	∼C_{2v}: $^1B_2$
μ	5.4	7.4	8.0
N_1-C_1	139.7	135.5	133.8
C_1-C_2	138.7	144.4	142.5
C_2-C_3	144.6	144.8	141.1
C_3-C_4	146.9	138.6	141.3
C_4-C_5	141.6	145.0	143.7
C_5-N_2	114.0	113.6	114.0
$C_2C_1N_1H_3$	26.9°	0.0°	0.0°
θ	43.9°	0.0°	0.0°
Σ(N-angle)	339.0°	360.0°	360.0°

[a] This work. [b] Reference 25.

Table 4. Locally Excited (LE)-State Geometries for DMABN: Point Group and State Symmetries, Dipole Moments μ (in D), Bond Lengths (in pm), Pyramidalization Angle θ (Chart 1), and Sum of Bond Angles at the Amino Nitrogen Atom

	CAS(4e,4o)/6-31G(d)		AM1-CAS (6e/5o), LE (planar)[b]	AM1-CISD (6e,6o), LE (planar)[c]
	LE (pyramidal)[a]	LE (planar)[a]		
symmetry	C_s: 1 A″	C_{2v}: $^1B_2$	C_{2v}: $^1B_2$	C_{2v}: $^1B_2$
μ	6.0	9.6	8.0	
N_1-C_1	139.3	136.9	136.6	136.5
C_1-C_2	139.5	143.2	143.3	141.5
C_2-C_3	144.6	144.8	140.4	140.5
C_3-C_4	146.5	138.4	141.3	141.5
C_4-C_5	141.5	145.0	141.5	142.2
C_5-N_2	114.1	113.7	116.2	116.1
N_1-C_6	144.8	145.6	144.4	
$C_2C_1N_1C_6$	15.4°	0.0°	0.0°	0.0°
θ	25.0°	0.0°	0.0°	0.0°
Σ(N-angle)	353.3°	360.0°	360.0°	360.0°

[a] This work. [b] Reference 33. [c] Reference 27.

Computed dipole moments can be compared with those reported by Schuddeboom et al.[13] in 1,4-dioxane solution. The computed dipole moment of 6.0 D for ABN is only slightly smaller than the experimental value of 6.6 D, whereas the dipole moment of 6.6 D for DMABN matches the experimental value exactly. The fact that the applied CASSCF method is able to reproduce the experimentally determined pyramidal character of the ground-state molecules validates this method as an adequate approach to describe a possible change of pyramidalization toward planarization in excited states.

3.2. Locally Excited States. For both ABN and DMABN, pyramidal as well as planar LE states have been localized by geometry optimization (Figures 1 and 2, Tables 3 and 4). In both molecules the respective structures exhibit similar characteristics. The pyramidal states belong to the 1A″ representation in C_s symmetry and the planar states to the $^1B_2$ representation in the C_{2v} point group. However, these representations transform into each other, so that both states correspond to local minima on the L_b-type potential energy surface. In both cases the $S_1 \rightarrow S_0$ transition is calculated to be short-axis polarized, in agreement with the experiment. In the case of ABN, an imaginary frequency corresponding to a b_1 symmetric in-plane deformation mode has been detected. However, this imaginary frequency disappears without affecting the geometry to a noticeable extent when a different basis set (cc-pVDZ) is used, in agreement with observations from CIS calculations reported by Lommatzsch and Brutschy.[25]

For pyramidal conformations the geometry changes upon excitation are predominantly localized in the benzonitrile moiety. The degree of pyramidalization and the dipole moments remain basically unchanged. Instead, in the planar structures the aniline part experiences structural reorganization and the dipole moments are moderately increased.

In the pyramidal structures the C_2-C_3 and C_3-C_4 bonds are considerably expanded and the cyano group steps into conjugation with the neighboring C_4-C_5 bond. The magnitude of pyramidalization of the amino groups is slightly increased by 2−3° and the dipole moments of both molecules decrease by 0.6 D with respect to the ground state.

In the planar structures the phenyl−amino bond (C_1-N_1) gains partial double-bond character, leading to a moderately increased conjugation and a partial charge transfer between the amino group and the benzene ring (Tables 3 and 4). The benzene bonds adjacent to the amino group as well as the central benzene bond lengths extend noticeably. The nitrile part is barely affected. Consequently, the planar LE states exhibit increased dipole moments of 7.4 D for ABN ($\Delta\mu = +1.4$ D with respect to S_0) and 9.6 D for DMABN ($\Delta\mu = +3.0$ D). For the LE state of DMABN, the calculated dipole moment is in agreement with the experimental value of 9−10 D, whereas for ABN this dipole moment is noticeably smaller than the reported experimental value of 8.0 D (in cyclohexane).[13]

The difference between pyramidal and planar structures arises from varying contributions of the single excitations a' ($5b_1$) → a'' ($3a_2$) (pyramidal, ABN = 44%, DMABN = 42%; planar, ABN = 73%, DMABN = 83%) and a'' ($2a_2$) → a' ($6b_1$) (pyramidal, ABN = 31%, DMABN = 32%; planar, ABN = 11%, DMABN = 6%) to the LE-state wave functions (cf. Figure 3). In ABN, the highest occupied molecular orbital ($5b_1$) is largely localized in the benzene ring, whereas in DMABN it is more concentrated on the amino nitrogen. Thus, single excitations from this orbital into the $3a_2$ antibonding orbital exhibit CT character, which is stronger in DMABN than in ABN.

Similar planar LE states have been described previously on the basis of ab initio CIS calculations[25] for ABN (Table 3) and semiempirical AM1-CI calculations for DMABN (Table 4).[27,33] These results slightly deviate from ours in the fact that the central C_2-C_3 bond is less expanded and the C_3-C_4 bond is slightly increased instead of decreased. Planar excited states have also been reported for aniline on the basis of CIS/6-31+G(d) calculations.[53−55] It was shown that the inclusion of diffuse basis functions results in quinoid-like structures, whereas omission of diffuse functions leads to expanded central C_2-C_3 bonds, in accordance with results from the present study.

3.3. Charge-Transfer States. TICT. It was shown by previous calculations that the shape of the adiabatic L_a-type potential energy surface along the twist coordinate strongly depends on the level of theory such that the lowest energy occurs either at planar[33] or perpendicular[24,34] structures or at intermediate twist angles.[20,21,24,26] Irrespective of the level of theory, all calculations agree in the fact that the dipole moment rises with increasing twist angle. This strongly suggests that, in polar solution, perpendicular or at least close to perpendicular structures are populated.[33,34] At the CAS(6e/5o) level employed in this work, the 90° twisted structure corresponds to a true minimum on the potential energy surface, as confirmed by vibrational analysis (Figure 2, Table 5). This is in agreement with calculations of Sobolewski and Domcke.[24]

Table 5. 90°-Twisted Charge Transfer (TICT) Excited-State Geometries for DMABN (L_a-type, C_{2v}: $1A_2$): Dipole Moments μ (in D) and Bond Lengths (in pm)

	CAS(6e,5o)/ 6-31G(d)[a]	CIS/ 3-21G[b]	INDO/1 ROHF[c]	AM1-CISD(6e,6o)[d]
μ	15.6	13.5		14.8
N_1-C_1	143.3	134.4	142.6	133.1
C_1-C_2	142.3	146.8	146.2	144.3
C_2-C_3	136.1	135.0	143.3	142.2
C_3-C_4	142.9	141.3	145.1	145.3
C_4-C_5	141.7	140.7	144.9	147.0
C_5-N_2	114.5	114.7	128.8	117.5
N_1-C_6	145.7	147.6	143.4	

[a] This work. [b] Reference 22. [c] Reference 32. [d] Reference 27.

The electronic wave function of the TICT state ($1A_2$) is fully characterized by a single excitation from the localized amino nitrogen lone pair orbital (b_2) to the b_1 π^* orbital located entirely in the benzonitrile moiety (cf. Figure 3). However, the $A_2 \rightarrow A_1$ transition is symmetry forbidden, so no fluorescent emission is expected for the perpendicular configuration. Two reasons explaining the experimentally observed fluorescence have been put forward: either vibronic coupling with an a_2 symmetric normal mode is operative or fluorescence occurs before the perpendicular twist is reached.[24] The dipole moment of 15.6 D calculated here coincides with known experimental data (15−16 D).[13]

The structure of the TICT state has been analyzed before by various groups. The benzene ring of the TICT state calculated here exhibits a quinoidal conformation, in agreement with CIS/3-21G calculations.[22] On the AM1-CISD level, the quinoidal pattern is less pronounced.[27] The cyano bond length (C_5-N_2, Table 5) increases slightly. In contrast to CIS/3-21G[22] as well as AM1-CISD[27] calculations, the phenyl−amino bond as found in this work is enlarged by 4.7 pm with respect to the ground state (N_1-C_1, Tables 2 and 5). A comparatively long phenyl−amino bond in the TICT state was also obtained by Broo and Zerner using low-level INDO/1-ROHF calculations.[32] An elongation has important consequences for the frequency shift of the phenyl−amino stretching vibration (ν(PhN)) in the CT state. Knowing the frequency shift of this mode is crucial to distinguish between the TICT and PICT models (cf. Section 4.1). Therefore, a clarification of this discrepancy is indispensable here.

First, it has been verified that the elongation is neither a consequence of the small active space chosen for geometry optimization nor of the basis set by performing single-point calculations along the stretching coordinate with an expanded active space (12e/11o, cf. Section 2) and larger basis sets (6-31+G(d), 6-311G(d,p)). The elongation is reproduced correctly.

Furthermore, the elongation is not easily predicted from qualitative molecular orbital arguments. Figure 3 shows a molecular orbital correlation diagram for nontwisted (planar or pyramidal) and perpendicular structures. The pure benzene b_1 and the amino nitrogen lone pair p_z orbital combine to a bonding ($4b_1$ in C_{2v}) and an antibonding ($5b_1$ in C_{2v}) orbital with respect to the phenyl−amino bond. Both are doubly occupied in the wave function of the electronic ground-state minimum. Upon twisting, the $4b_1$ orbital develops into the nonbonding $7b_1$ benzene orbital and the $5b_1$ orbital correlates with the nonbonding p_y amino nitrogen lone pair orbital ($10b_2$), which is singly occupied in the TICT state wave function. The remaining

(53) Jiang, J. C.; Lin, C. E. *J. Mol. Struct. (THEOCHEM)* **1997**, *392*, 181−191.
(54) Tzeng, W. B.; Narayanan, K.; Shieh, K. C.; Tung, C. C. *J. Mol. Struct. (THEOCHEM)* **1998**, *428*, 231−240.
(55) Sinclair, W. E.; Pratt, D. W. *J. Chem. Phys.* **1996**, *105*, 7942−7956.

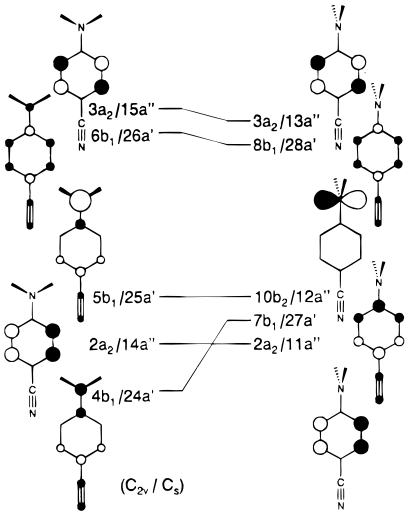

Figure 3. Qualitative molecular orbital correlation diagram between nontwisted (planar or pyramidal) DMABN and perpendicular structures.

electron occupies the $8b_1$ benzene orbital, which is also nonbonding with respect to the phenyl−amino bond. Overall, both bonding and antibonding interactions in the electronic ground state develop completely into nonbonding interactions in the TICT state. Thus, the prediction of a bond length change in the TICT state depends on the degree of bonding and antibonding interactions in the ground state.

Finally, comparison of X-ray crystal structure bond lengths for twisted and nontwisted ground-state structures of miscellaneous aminobenzonitriles reported by Heine et al.[52] might provide some insights. Whereas the measured phenyl−amino bond lengths for nontwisted aminobenzonitriles indicate some double-bond character (136.4···137.0 pm, cf. Tables 1 and 2), the partially twisted (59.3°) 3,5-dimethyl-4-(dimethylamino)-benzonitrile exhibits a bond length of 141.4 pm.[52] This more pronounced single bond is mainly attributed to the reduced delocalization of the nitrogen lone pair into the aromatic ring and, therefore, confirms the elongation of the phenyl−amino bond calculated here for the TICT state. It is concluded that the CASSCF method describes the change of the phenyl−amino bond length correctly, whereas the CIS and AM1 methods seem to have some deficiencies.

PICT. A planar CT state is reached by optimizing the $2A_1$ state, which corresponds to the second excited state at the ground-state minimum as well as at the relaxed geometry. The electronic wave function of the PICT state is predominantly (≈81%) described by the single excitation $5b_1 \rightarrow 6b_1$ (cf. Figure 3). The double excitation $1a_2,5b_1 \rightarrow 6b_1,2a_2$ and single excitation $1a_2 \rightarrow 2a_2$ have minor contributions.

The geometry of the planar charge-transfer state has a quinoidal conformation with partial double-bond character in the phenyl−amino bond (Figure 2, Table 6). The aromatic bonds adjacent to the substituents are elongated, whereas the central aromatic bonds are shortened. The phenyl−cyano bond is in conjugation with the cyano bond and hence reduced, whereas the cyano bond itself is enlarged. The dipole moment of 13.1 D calculated here is only slightly smaller than the experimentally observed value of 15−16 D.[13] Because the dipole moment of the S_1 state ($1B_2$) in the PICT geometry amounts to only 7 D, it is conceivable that polar solvation stabilizes the PICT state ($2A_1$) more than the $1B_2$ state, which might interchange their energetic order at the PICT geometry.

Although not explicitly assigned to the PICT model, accordant structures have already been reported on the semiempirical AM1-CI level.[27,33] The geometries of these states are quite similar to the one obtained in this work (Table 6), but the AM1 dipole moment of 10.5 D is appreciably smaller than that calculated by the CASSCF method (13.1 D).

Table 6. Planar Charge Transfer (PICT) Excited-State Geometries for DMABN (L_a-type, C_{2v}: $2A_1$): Dipole Moments μ (in D) and Bond Lengths (in pm)

	CAS(4e,4o)/ 6-31G(d)[a]	AM1-CAS(6e,5o)[b]	AM1-CISD(6e,6o)[c]
μ	13.1	10.5	12.5
N_1-C_1	135.1	137.9	138.5
C_1-C_2	143.8	144.1	144.6
C_2-C_3	138.5	137.9	138.1
C_3-C_4	144.8	142.2	141.8
C_4-C_5	140.2	140.4	141.2
C_5-N_2	115.1	116.6	116.7
N_1-C_6	145.3	143.7	

[a] This work. [b] Reference 33, μ value in acetonitile. [c] Reference 27.

Table 7. Rehybridized Charge Transfer (RICT) Excited-State Geometries for DMABN (L_a-type, C_s: $1A''$): Dipole Moments μ (in D) and Bond Lengths (in pm)

	CAS(4e,4o)/6-31G(d)[a]	CIS/3-21G[b]
μ	13.8	16.4[c]
N_1-C_1	134.0	135.5
C_1-C_2	143.0/143.1	141.5/141.6
C_2-C_3	135.7/135.4	136.4/136.5
C_3-C_4	142.2/143.0	140.2/140.7
C_4-C_5	143.0	142.4
C_5-N_2	124.9	129.8
N_1-C_6	145.7/145.8	146.6
$C_4C_5N_2$	125.4	126.4

[a] This work. [b] Reference 22. [c] CASSCF/DZP//CIS/3-21G value.

RICT. The optimized geometry of the RICT state is comparable to the one obtained by Sobolewski and Domcke at the CIS/3-21G level (Table 7).[22] The quinoidal pattern of the benzene ring is slightly more pronounced at the CASSCF level, and the cyano bond is somewhat shorter. The calculated dipole moment of 13.8 D is smaller than that at the CIS/3-21G level (16.4 D). The electronic wave function is dominated by the excitation a'' (π) → a' ($\pi_{CN,yz}$*), again in agreement with previously published results (cf. Figure 3).[22]

4. Discussion

4.1. Vibrational Analysis. Excited-state vibrational spectra have been calculated for all theoretical model structures under consideration: the planar and pyramidal LE states for ABN and DMABN and the TICT, PICT, and RICT models for DMABN. They exhibit different characteristics such that a comparison of experimental and theoretical data makes it possible to evaluate the theoretical models. The normal modes, which are largely localized as stretching motions of the cyano and phenyl−amino bonds, hereafter abbreviated as ν(CN) and ν(PhN), play a prominent role in the discrimination of the respective models. Infrared data are compiled in Tables 8 and 9 for ABN and DMABN, respectively. In Figure 4 experimental and calculated frequencies and intensities of the ν(CN) and ν(PhN) modes are compared for the LE state of ABN. Figures 5 and 6 depict corresponding results for the LE and CT states of DMABN, respectively. Frequency and intensity changes from the ground to excited states are denoted by dashed arrows. Absolute experimental intensities have been scaled to match the calculated values. Other strongly infrared active vibrational modes, such as aromatic skeletal stretching or methyl and amino group (for ABN) deformation modes, are not distinctive for the different

Table 8. ABN: Experimental and Calculated (Scaled by 0.9) Harmonic Frequencies ν (in cm^{-1}), Frequency Shifts $\Delta\nu$ (in cm^{-1}) between S_0 and LE State, Absolute Intensities I (in km mol^{-1}) for the Ground State, and Intensity Changes ΔI between S_0 and LE State

	ν (CN)			ν (PhN)		
	ν	$\Delta\nu$	I, ΔI	ν	$\Delta\nu$	I, ΔI
experimental[a]						
S_0	2216	-	23	1317		15
LE	2218	+2	−44%	1313	−4	−17%
calculated						
S_0	2353	-	74	1265		61
LE pyramidal	2323	−30	−30%	1254	−11	−25%
LE planar	2349	−4	−93%	1306	+41	−79%

[a] Reference 41.

Table 9. DMABN: Experimental and Calculated (Scaled by 0.9) Harmonic Frequencies ν (in cm^{-1}), Frequency Shifts $\Delta\nu$ (in cm^{-1}) between S_0, LE, and CT States, Absolute Intensities I (in km mol^{-1}) for the Ground State, and Intensity Changes ΔI between S_0, LE, and CT States

	ν (CN)			ν (PhN)		
	ν	$\Delta\nu$	I, ΔI	ν	$\Delta\nu$	I, ΔI
experimental[a]						
S_0	2215		44	1373		38
LE	NO[b]	NO	−100%	NO	NO	−100%
CT	2112	−103	+50%[c]	NO	NO	−100%
calculated						
S_0	2352		85	1356		134
LE pyramidal	2372	+20	+76%	1352	−4	−40%
LE planar	2323	−29	−94%	1373	+17	−95%
TICT	2242	−110	+175%	1286	−70	−75%
PICT	2316	−36	+260%	1403	+47	−50%
RICT	1552	−800	+353%	1395	+39	+127%

[a] Reference 41. [b] Not observed [c] After 15 ps, ref 41.

LE and CT models and were considered, therefore, only to determine the scaling factor between experimental and calculated intensities.

Good agreement between theoretical and experimental data for the ν(CN) and ν(PhN) modes is obtained in the ground state. The strength of the cyano bond is somewhat overestimated by the calculation (cf. Section 3.1), which causes the vibrational frequencies to be systematically too high by about 140 cm^{-1} when the standard scaling factor of 0.9 is used. This does not, however, affect relative frequency shifts between the ground and excited states, as explained above.

The transient infrared spectrum of ABN has been assigned to the LE state.[41] Only small frequency and intensity changes upon excitation have been observed experimentally. This pattern is best reproduced by the infrared spectrum calculated for the pyramidal LE structure (Figure 4, top). The small frequency and intensity changes calculated for the ν(PhN) mode and the intensity change for the ν(CN) mode are in very good agreement with the experimental observation. Solely the calculated frequency shift for the ν(CN) mode is somewhat overestimated. For the planar LE state of ABN (Figure 4, bottom), large intensity reductions for both modes and a considerable upshift for ν(PhN) are predicted, which is in contradiction to the experimental result. Therefore, the LE state of ABN has a pyramidal structure in acetonitrile. This concurs with structural information obtained from rotationally resolved fluorescence spectroscopy.[39]

For DMABN, the transient infrared spectrum for the LE state (Figure 5) is noticeably different, and so must be its structure.[41] The intensity of the ν(PhN) and ν(CN) modes vanishes completely. Therefore, the assignment of a certain structure can

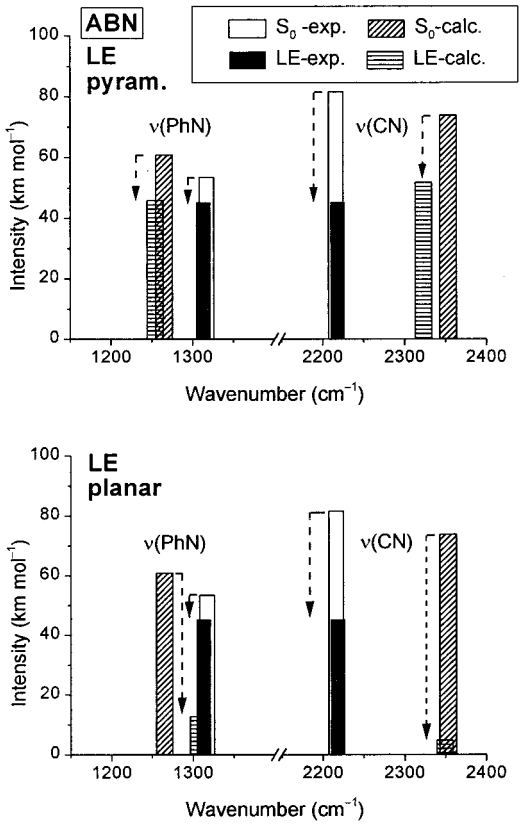

Figure 4. Experimental and calculated (scaled by 0.9) vibrational frequencies and intensities (experimental data are scaled) for the ν(PhN) and ν(CN) modes in the LE state of ABN. Top: theoretical data for the pyramidal LE state. Bottom: theoretical data for the planar LE state (see text). Arrows denote changes between the ground and excited states.

be based only on intensity changes. The infrared spectra calculated for the pyramidal and planar LE states of DMABN exhibit a pattern similar to that of the respective spectra for ABN. The infrared spectrum for the pyramidal LE state shows a moderate decrease in intensity for the ν(PhN) mode and even an increase for the intensity of the ν(CN) mode, in contrast to the experiments. Unlike the pyramidal structure, the planar one has strongly reduced intensities for both modes matching the experimental infrared spectrum. Accordingly, the LE state of DMABN is planar in solution. This was also indicated by recent gas-phase experiments.[38]

A new infrared absorption band appears on a time scale of 4 ps for DMABN dissolved in acetonitrile.[41] This band has been attributed to the ν(CN) mode in the CT state, which is downshifted by 103 cm^{-1} with respect to the ground state. After 15 ps the band intensity is about 50% larger than in the ground state. A band corresponding to the ν(PhN) vibrational mode in the CT state was not detected. Calculated infrared spectra for the TICT, PICT, and RICT models are shown in Figure 6, together with experimental data. For the RICT model (Figure 6, bottom), an enormous downshift of 800 cm^{-1} for the ν(CN) mode is calculated, reflecting the conversion of the cyano triple bond into a bent double bond.[22−24] This is clearly in contradiction to the observed downshift of 103 cm^{-1}. Furthermore, a considerable increase in intensity is predicted for the ν(PhN) mode, again in contradiction to the experiment. Therefore, the RICT model is definitely ruled out as a CT mechanism in DMABN.

The frequency shifts calculated for the ν(PhN) vibrational mode differ qualitatively for the TICT (Figure 6, top) and PICT

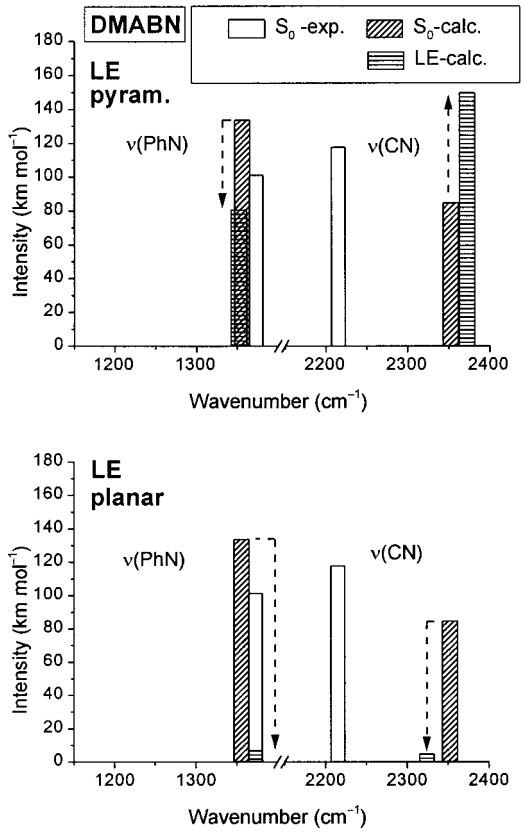

Figure 5. Experimental and calculated (scaled by 0.9) vibrational frequencies and intensities (experimental data are scaled) for the ν(PhN) and ν(CN) modes in the LE state of DMABN. Top: theoretical data for the pyramidal LE state. Bottom: theoretical data for the planar LE state (see text). Arrows denote changes between the ground and excited states.

(Figure 6, middle) models. Within the TICT model, the phenyl−amino bond is expanded, which causes the vibrational frequency to be downshifted by 70 cm^{-1}. In contrast, the phenyl−amino bond in the PICT state exhibits partial double-bond character and is upshifted by 47 cm^{-1}. In both cases, a marked decrease in intensity is calculated. This concurs with the experimental observation, as the intensity of the ν(PhN) mode in the CT state was below the detection limit. Thus, a distinction of the TICT and PICT models based upon experimental results for the ν(PhN) mode is prevented.

Interestingly, the downshift of the ν(CN) band differs for both models. For the TICT model a downshift of 110 cm^{-1} is calculated, whereas the predicted downshift for the PICT state is only 36 cm^{-1}. The downshift for the TICT model is very close to the experimental observation of 103 cm^{-1}, whereas the shift for the PICT model is too small. For both models, a band intensity increase in qualitative agreement with experimental data is calculated. Therefore, the calculated downshift for the ν(CN) mode appears to be in favor of the TICT model, but, taking the accuracy of the theoretical model into account, it does not seem to be warranted to consider this individual argument as final proof.

4.2. ICT Mechanism. Comparison of calculated excited-state and femtosecond transient infrared spectra[41] leads to the conclusion that the LE state in DMABN is planar, whereas the LE state in ABN is pyramidal just as for both ground states. The RICT model is reliably excluded as an ICT mechanism. A definite distinction between the TICT and PICT models is not possible yet, although the vibrational pattern analysis favors the TICT process.

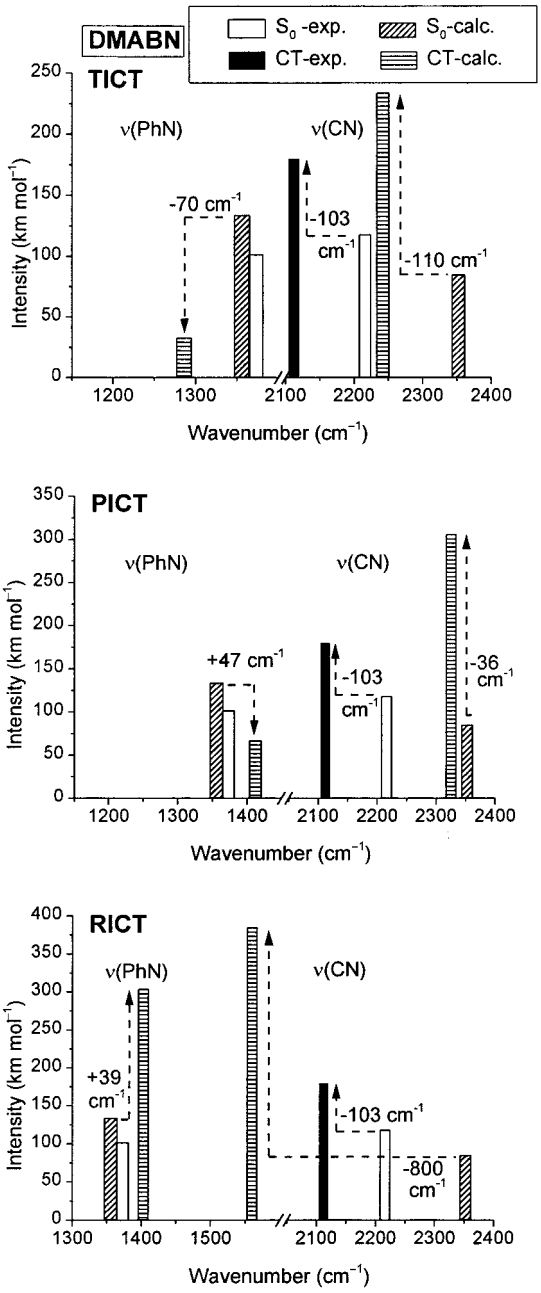

Figure 6. Experimental and calculated (scaled by 0.9) vibrational frequencies and intensities (experimental data are scaled) for the ν(PhN) and ν(CN) modes in the CT state of DMABN. Top: theoretical data for the TICT model. Middle: theoretical data for the PICT state. Bottom: theoretical data for the RICT state (see text). Arrows denote changes between the ground and excited states.

The following ICT mechanism emerges from the present results. Initially the polar $2A'$ ($2A_1$) S_2 state of the pyramidal ground-state molecule is excited, the transition being more strongly allowed than the excitation to the lower lying $1A''$ ($1B_2$) S_1 state. Subsequently, internal conversion populates the $1B_2$ LE state, which is the lowest excited state at the respective geometry, and gives rise to the experimentally observed normal fluorescence. In acetonitrile, the LE state is formed in less than 500 fs.[41] The conversion of the LE to the CT state occurs with a time constant of 4 ps in acetonitrile.[41] This rate constant can be compared to theoretical predictions deduced by Kim and Hynes from a two-dimensional model of the twist motion and a solvent coordinate,[36] which accounts for nonequilibrium solvation. Within this model the time constant of 4 ps corre-

sponds to a conversion along the TICT coordinate with an equilibrated solvent. Earlier time-resolved fluorescence measurements with substantially lower time resolution gave a value of 6 ± 1 ps,[16,18] which would have suggested some participation of nonequilibrium solvation in the reaction coordinate.

Planarization of the amino group in DMABN takes place between the vertical excitation and the formation of the LE state. This excludes planarization or the inversion motion, respectively, as the rate-determining step in the ICT formation and relevant reaction coordinate connecting the LE and CT states as proposed by the pseudo-Jahn−Teller model.[12−17] In fact, as has been noticed before,[20] the inversion mode is of a' (b_1) symmetry and cannot couple the L_b-type $1A''$ ($1B_2$) LE and the L_a-type $2A'$ ($2A_1$) PICT states. Instead, suitable coupling modes must be of a'' (b_2) symmetry, which corresponds to in-plane deformation modes. In support of this symmetry argument, it has been shown by CASPT2 calculations that the inversion mode is inactive as a coupling mode.[20,21] Consequently, the vibronic coupling mechanism of the pseudo-Jahn−Teller model based upon the inversion motion of the amino moiety is called into question. However, the existence of a planar CT state is not excluded. In fact, a planar CT state with a dipole moment of about 14 D has been identified as a local minimum on the L_a-type potential energy surface by individually optimizing the planar $2A_1$ state. This state might be reached along a suitable reaction coordinate by vibronic coupling with a'' (b_2) symmetric in-plane deformation modes.

Vibronic coupling is also a necessity for the TICT mechanism as long as C_2 symmetry is retained along the twisting reaction coordinate. The L_b-type (LE state) and the L_a-type (TICT state) potential energy surfaces must be coupled by *b* symmetric modes to enable a transition.

5. Summary

Ab initio CASSCF optimizations are performed for different models for the LE states of ABN and DMABN as well as the CT state of DMABN in order to analyze femtosecond transient infrared spectra.[41] The LE state of ABN is pyramidal, whereas the LE state of DMABN is planar. This has the important consequence that the inversion motion of the amino moiety cannot serve as reaction coordinate and rate-determining step in the ICT mechanism. Nevertheless, this does not rule out the PICT model, because a planar and highly polar state exists as a local minimum on the L_a-type potential energy surface in addition to the TICT and RICT states. The RICT model is reliably excluded as an ICT mechanism in DMABN, as the calculated frequency shift is far different from the experimentally observed one. Altogether, the results are in favor of the TICT mechanism, but a definite distinction between the TICT and PICT models based upon available experimental results is not possible. However, the calculations show that an experimental observation of the ν(PhN) vibrational frequency would allow for a final decision between TICT and PICT.

The combined approach of ultrafast vibrational spectroscopy and high-level excited-state calculations provides valuable new information. In the example studied, we were able to resolve the transients involved in the ICT reaction in DMABN. This method is generally suited to study dynamics of fast chemical reactions and the structures of transient species involved.

Acknowledgment. We thank T. Elsaesser, E. T. J. Nibbering, and K. A. Zachariasse for valuable discussions. J.D. gratefully acknowledges a fellowship of the Deutsche Forschungsgemeinschaft. Computer time has been kindly provided by the Weierstrass-Institute, Berlin.

Supporting Information Available: Energy diagram for DMABN (relative to S_0) at the CAS(12e/11o/6-31G(d) level; Cartesian coordinates and a table of total energies in hartrees for structures included in Figures 1 and 2 (PDF). This material is available free of charge via the Internet at http://pubs.acs.org.

JA992095E